THE EUROPEAN SOCIETY OF MEDICINE
Medical Research Archives, Volume 13 Issue 6

REVIEW ARTICLE

A Review of Pharmaceutical Powder Crystallography – Process, Results, and Applications

James A. Kaduk [1]

[1] Illinois Institute of Technology, 3101 S. Dearborn St., Chicago IL 60616, and North Central College, 131 S. Loomis St., Naperville IL 60540

OPEN ACCESS

PUBLISHED
30 June 2025

CITATION
Kaduk, JA., 2025. A Review of Pharmaceutical Powder Crystallography – Process, Results, and Applications. Medical Research Archives, [online] 13(6).
https://doi.org/10.18103/mra.v13i6.6600

DOI
https://doi.org/10.18103/mra.v13i6.6600

ISSN
2375-1924

ABSTRACT

In the absence of single crystals, powder diffraction data (especially synchrotron data) can provide a means of determining the crystal structure of an active pharmaceutical ingredient. The process of solving and refining a crystal structure using powder data is summarized, and suggestions for overcoming challenges are given for the various steps. Indexing can often be a bottleneck. Measures of the quality of a Rietveld refinement - including statistical, graphical, and chemical reasonableness (particularly the root-mean-square displacement between a Rietveld-refined and a DFT-optimized structure) - are described, and examples are given of what to expect, based on a large number of structures determined using synchrotron powder diffraction data. Recent crystal structures of important and/or interesting molecules are reviewed. Examples illustrating the accuracy which can be achieved, interesting features of the process of structure solution, the distinction between salts and co-crystals, and phase transitions are also reviewed.

Introduction

In this review of pharmaceutical powder crystallography, I provide recent (last five years) examples of its application – principally to salts/cocrystals and phase transitions, but also some important molecules. Because the field is fairly specialized, I feel it is important to quantify its scale, and to provide experience-based hints on what to expect and what can go wrong, for those who might want to join the field.

By "powder crystallography" I mean the solution and refinement of crystal structures using powder diffraction data, in contrast to the more-usual single crystal experiment and the use of powder diffraction for qualitative and quantitative phase analysis. It is still a good rule that "If you have a single crystal, you should use it.", but powder diffraction can be a useful "Plan B". Overlap of three dimensions of diffraction data into a one-dimensional powder pattern ultimately limits the information content, but powder diffraction can still be a powerful technique, especially when single crystals of a pharmaceutical active ingredient (API) are unavailable.

A search of the Inorganic Crystal Structure Database (ICSD)[1] for crystal structures flagged as "powder" indicates and increase from about 1200 to 3000/year over the last 45 years (Figure 1). Most of these represent new compositions which are isostructural to known compounds. Establishing which are truly new structures would require an entry-by-entry examination. A search for powder structures of organic compounds in the Cambridge Structural Database (CSD)[2] indicates an increase from about zero in 1990 to about 400-450/year currently (Figure 1).

The number of crystal structures in the CSD Drug Subset has increased from about 75/year in 1990 to about 900/year currently (Figure 2). The number of powder structures in the CSD Drug Subset is much smaller, at about 35/year (Figure 3). The spike in 2005 represents a variable-pressure study of glycine[3], and so is an outlier in the trend. Thus powder structures represent about 4% of those in the CSD Drug Subset (Figure 4). As seen from Figure 3, I myself account for a significant fraction of the total pharmaceutical powder structures. In the following discussion, I emphasize my own structures (as I have more information available), but cover the available universe. Most of my pharmaceutical structures have been part of a project with the International Centre for

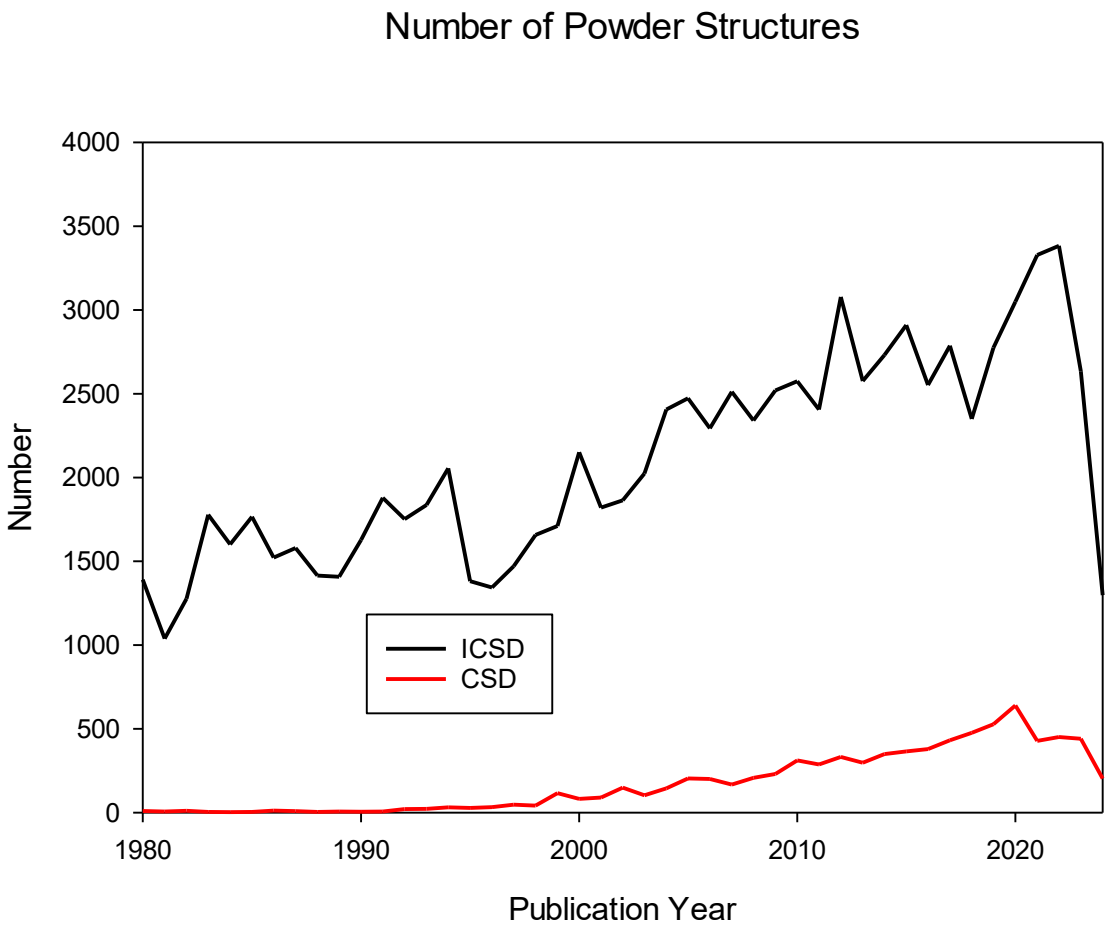

Figure 1. Number of powder crystal structures per year in the Inorganic Crystal Structure Database (black) and the Cambridge Structural Database (red).

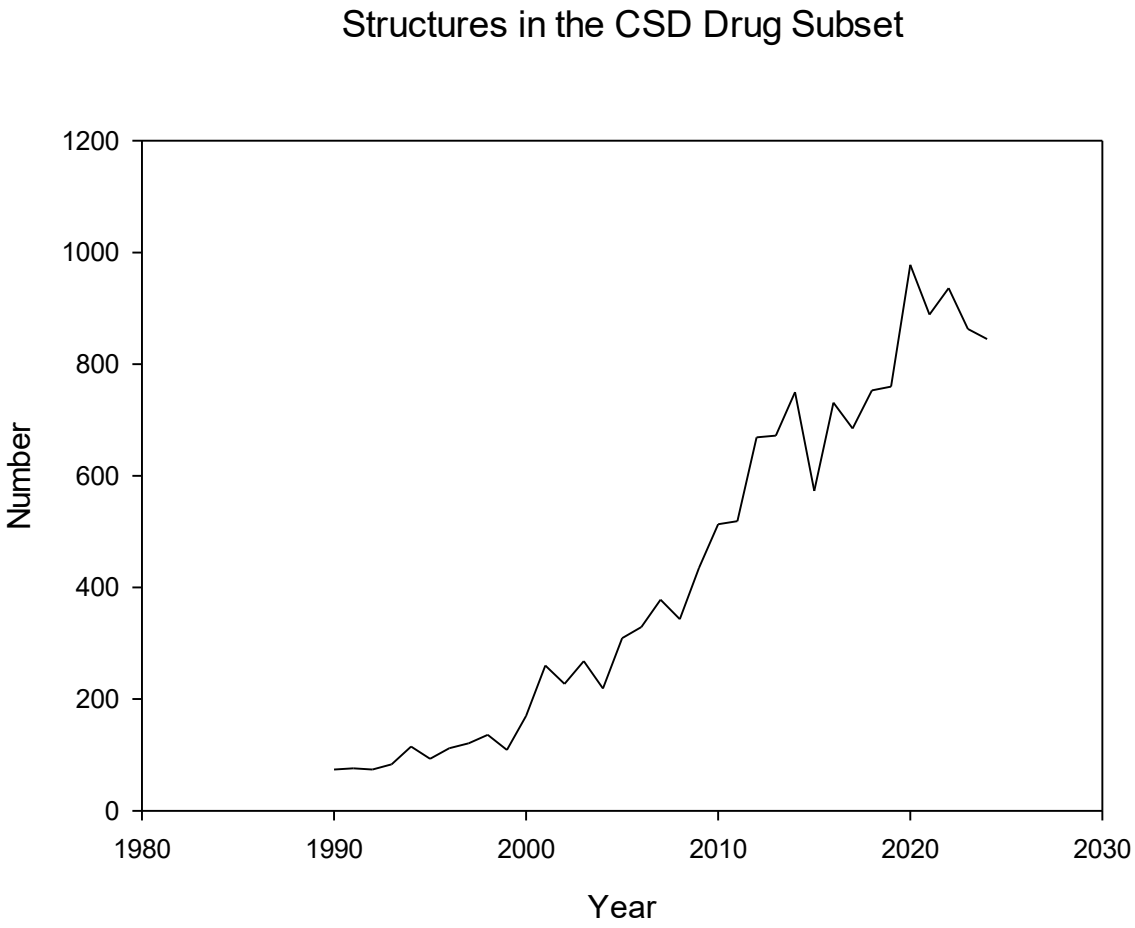

Figure 2. Number of crystal structures per year in the Cambridge Structural Database Drug Subset.

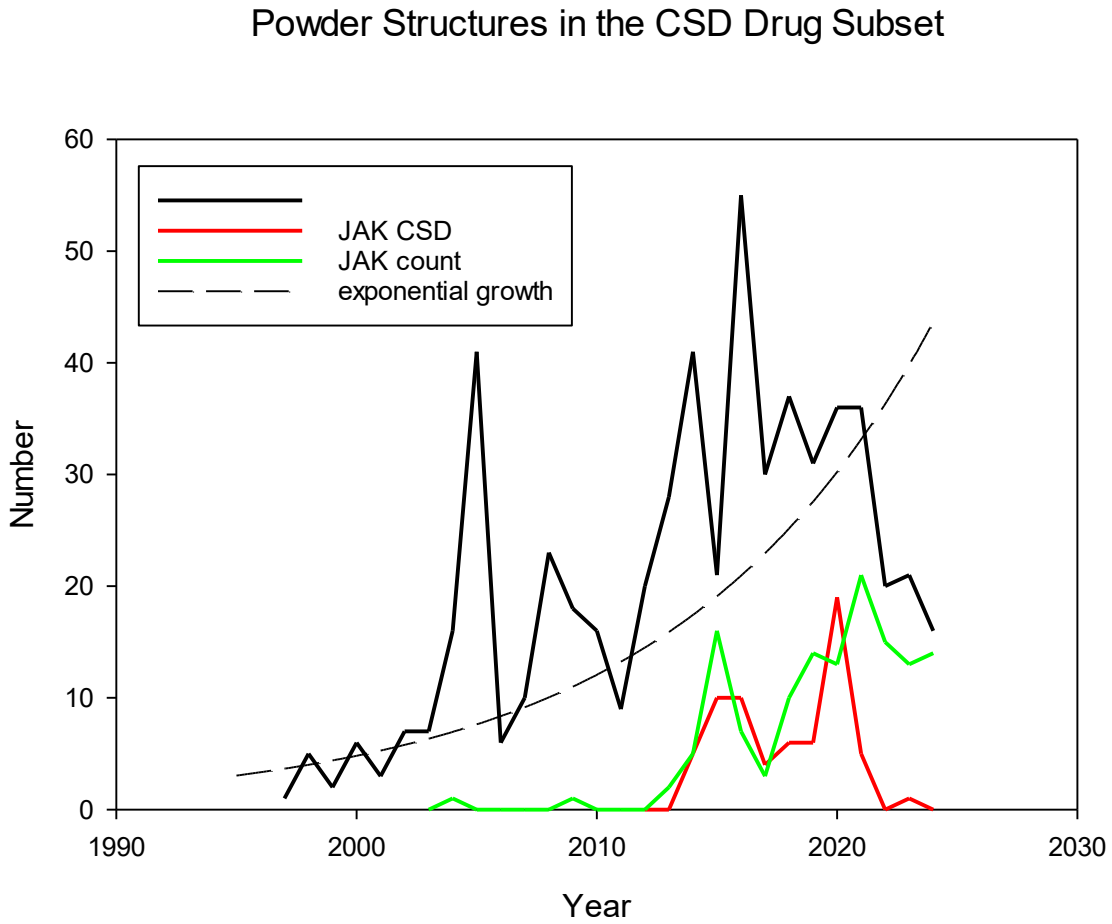

Figure 3. Number of powder crystal structures per year in the Cambridge Structural Database Drug Subset (black). The red line shows the number of structures by author = Kaduk, and the green line is my actual count. The black dashed line is an exponential growth to guide the eye.

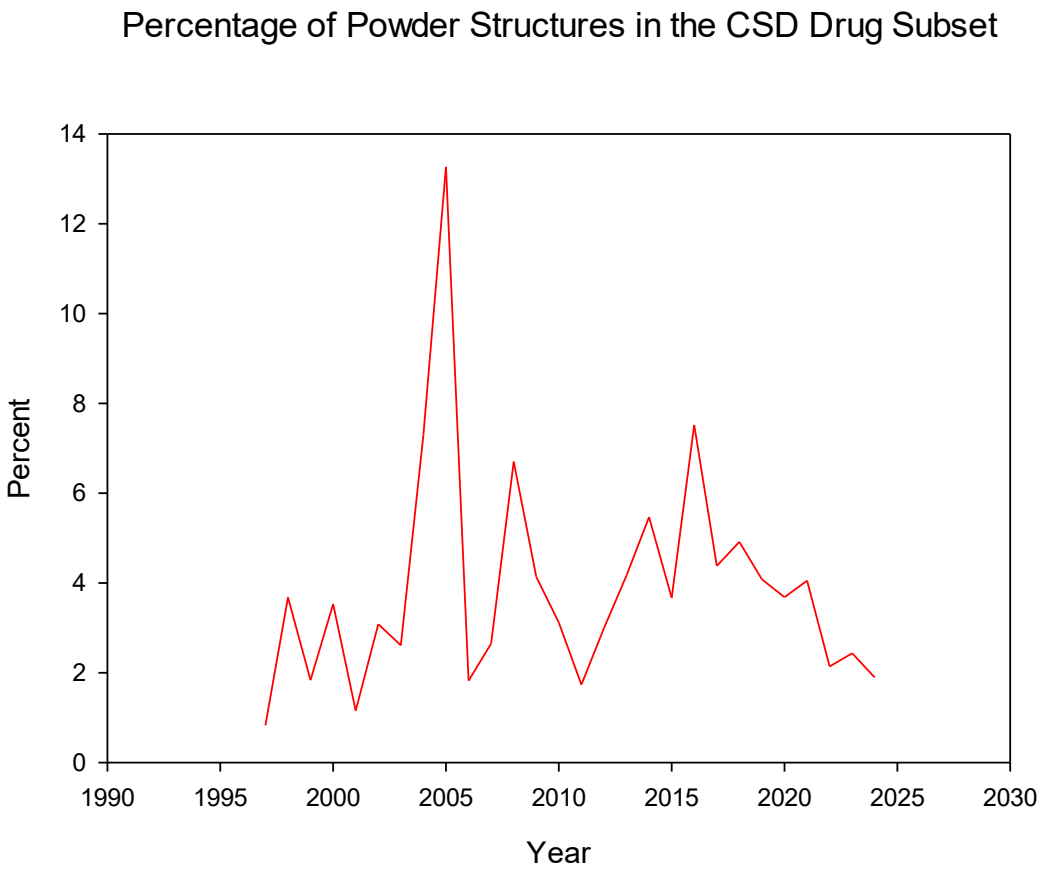

Figure 4. The percentage of powder structures per year in the Cambridge Structural Database Drug Subset.

Diffraction Data (ICDD). The project has two objectives: 1) to prepare high-quality powder patterns of large-volume commercial pharmaceuticals at ambient conditions to include in the Powder Diffraction File[4], and 2) to determine the crystal structures when they have not been reported. Most analytical powder diffraction is done at room temperature. When a single crystal structure exists, it was often done at low temperature (often 100K). Thermal expansion between 100 and 300K typically 1.0-1.5%, often anisotropic) shifts the peaks in a powder pattern (Figure 5) enough that those in a pattern calculated from a 100K structure will fall outside the normal windows used in a search/match (phase identification). So, even if such a calculated pattern exists in the PDF, the identification can be missed. Surprisingly many pharmaceutical crystal structures are unpublished, presumably because the innovator companies have kept them as trade secrets. Availability of the crystal structure permits quantitative phase analysis by the Rietveld method, avoiding the need for a pure reference sample necessary for PONKCS analyses[5].

Steps in the Process and Advice on What to Expect

The process of solving a crystal structure from powder data is conveniently visualized by "The Maze" (Figure 6), originally by Baerlocher and McCusker[6] and modified by David[7]. The characteristics of the sample are mostly beyond the scope of this review, but the sample should ideally be a single-phase fine-grained randomly oriented powder.

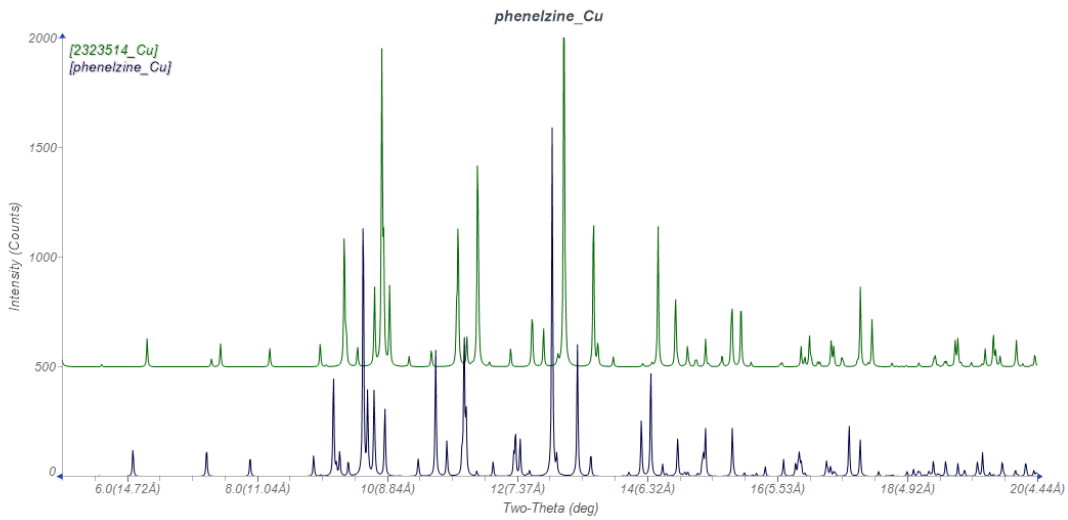

Figure 5. A calculated powder pattern (Cu K_α wavelength) for the 298K structure of phenelzine sulfate (black) and one calculated from the 80K structure of the same compound (green).

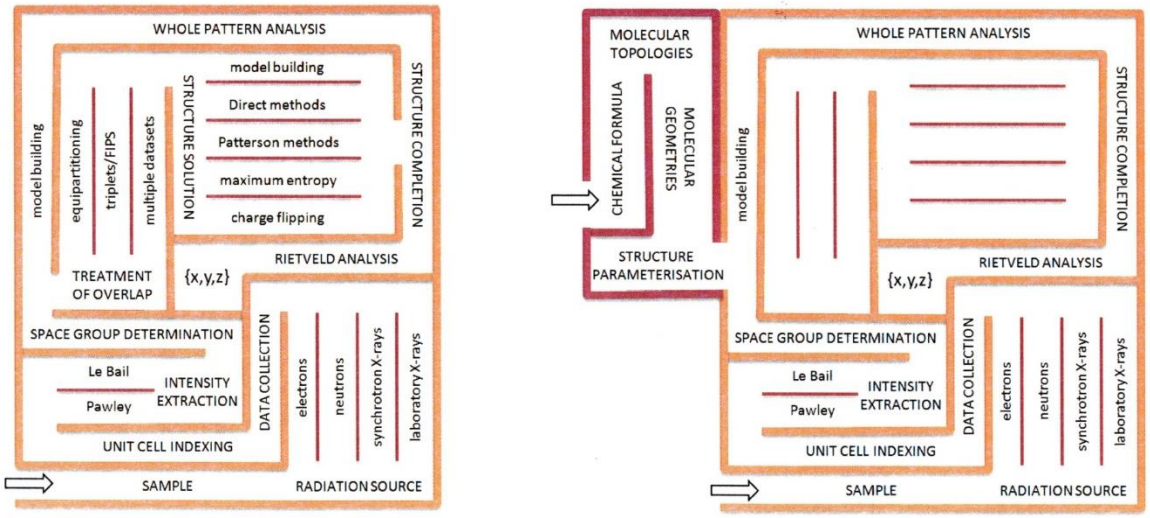

Fig. X.Z.1.1. (*a*) The maze of strategies associated with the determination of crystal structures from powder diffraction data (after Baerlocher & McCusker, 2002) and (*b*) the modified "global optimisation" maze showing the double start point and simplification of the principal maze.

Figure 6. See caption above. Figure 4.3.1 from International Tables for Crystallography Volume H. Reproduced with permission from the Internatioanl Union of Crystallgraphy, https://it.iucr.org.

For our purposes, we are considering X-ray powder diffraction, so there are two choices of radiation source: laboratory diffractometers and synchrotrons. Laboratory diffractometers (generally using Cu K_α radiation, though other wavelengths are occasionally used) are convenient, and often "good enough"; I have solved many organic crystal structures using laboratory data, even from a benchtop instrument.

Powder patterns of organic samples measured on a laboratory diffractometer using the typical Bragg-Brentano (flat plate) configuration can be prone to systematic errors, which complicate the structure solution process. The two major errors are specimen transparency (which shifts the peaks to lower angles) and specimen displacement (which most often shifts the peaks to higher angles, when the surface of the specimen is too high). Transparency also generates extra peak asymmetry and broadens the peaks compared to those from an inorganic sample, but the main concern is the shift in peak positions.

The use of synchrotron radiation offers advantages in resolution (peak widths), signal/noise, and peak/background. Synchrotron patterns do not suffer from transparency and displacement errors. We normally emphasize the improved resolution (which always helps), but few pharmaceutical samples exhibit the instrumental resolution, since they suffer from microstrain broadening. Thus, the highest resolution synchrotron beamline is not always necessary. The best synchrotron beamline is the one you can get time on! The complexity of pharmaceutical powder problems means that one can often waste time trying to obtain a structure from laboratory data; the process is generally more efficient at a synchrotron, so why handicap yourself with less than the best data? An unspoken disadvantage of synchrotron radiation for pharmaceutical samples is beam damage. Most of the pharmaceutical samples I have measured show subtle or not-so-subtle signs of changes during the measurement: shifts in peak positions and shapes, which can complicate structure solution and refinement. My synchrotron powder data on pharmaceuticals have been collected at 11-BM at the Advanced Photon Source at Argonne National Laboratory and the Canadian Light Source. There are other comparable synchrotrons around the world.

Indexing a powder pattern (determining the lattice constants = unit cell parameters) can be a bottleneck in structure solution. Indexing is all about accurate peak positions, so the systematic errors in a laboratory pattern must be minimized/eliminated by careful specimen preparation and/or use of an internal standard. Synchrotron patterns do not suffer from these errors, and so are easier to index. The higher resolution also helps in determining accurate positions of closely spaced or overlapping peaks. Impurity peaks are the bigger problem; if a synchrotron pattern cannot be indexed, it is almost a sure sign that the sample is a mixture. Attempting to describe the peak positions in a mixture by a single unit cell is a fruitless exercise. Weak impurity peaks can sometimes be tolerated, but if they are among the lowest-angle peaks (the most important ones for indexing) they can cause difficulties. Permitting a small number of unindexed lines is often a good strategy to overcome such difficulties.

Processing patent patterns can be challenging. The latest USP[8] states that "The agreement in the 2θ diffraction angles between specimen and reference is expected to be withing 0.2° for the same crystal form, whereas intensities between specimen and reference may vary considerably due to preferred orientation effects." The variations in peak position arise mainly from specimen displacement and transparency. Systematic errors as large as 0.2° can be fatal for success in indexing.

Most indexing programs and structure solution packages contain space group interpreting/suggesting routines. These programs often work well, but sometimes the space

group can be ambiguous, and multiple space groups must be tried.

In general a prelude to structure solution is a Le Bail/Pawley fit of the pattern[9]. These are structure-less profile fits, done with the aim of generating a table of *hkl* for speeding up the structure solution, rather than using the whole pattern.

The next step is structure solution. A good current summary of structure solution methods is given in Rizzi et al.[10]. I have had most success with direct methods/charge flipping and Monte Carlo Simulated Annealing. My experience using synchrotron radiation is that about half of pharmaceutical structures solve straightforwardly (in the sense that the solution is suggested directly by a program), while the other half can require weeks or months of operator intervention.

Direct methods and charge flipping use the peak intensities (used to generate structure factor amplitudes) to generate phases for the structure factors. These methods are thus "unbiased" by any chemical knowledge (except the kinds of atoms present in the structure). They both require atomic-resolution data: accurate intensities at *d*-spacings as low as 1.3-1.0 Å (70-100° 2θ using Cu radiation). For most pharmaceuticals, this criterion is not met; the peaks do not go out to high-enough angles, and peak overlap limits the accuracy of intensity extraction. Even using synchrotron data, only about 13% of pharmaceutical structures are solved by direct methods. The percentage could certainly be improved with more effort, but it is often quicker to switch to Monte Carlo Simulated Annealing, and use the chemical information we have.

Most pharmaceutical powder structures are solved using Monte Carlo Simulated Annealing (or its relative, parallel tempering). This is an example of a global optimization method. We use our knowledge of the chemical connectivity of the molecule(s), and fix (or nearly fix) the bond distances and angles. The variables include three coordinates for the position of a fragment, three orientation angles, and the torsion angles in the molecule. The fragment(s) are placed in a fixed unit cell with known space group(s) in a random position, random orientation, and with random torsion angles. The powder pattern is calculated and compared to the experimental one. Then a "move" is made; one of the variables is changed, the pattern re-calculated and compared to experiment. If the agreement is poorer, the move is mainly discarded, but accepted with a finite probability which decreases throughout the process. If the agreement improves, the sequence of moves continues. Essentially this is a way of guessing the crystal structure, tens or hundreds of millions of times. The success rate is good up to about 30 variables, above which it decreases rapidly. But one only needs to succeed once! For any compound, there are many poor crystal structures. Plausible ones tend to occur at the bottoms of very deep and very narrow minima in a hypersurface. Such a global minimization technique provides a way of sampling all of these minima, and minimizing the chances of being trapped in a false minimum.

Structure refinement using powder diffraction data is carried out by the Rietveld method, using one of many available program packages. Although it is sometimes possible, it is uncommon to refine atom positions independently, as is the normal in a single crystal refinement. Even with synchrotron data, the molecules tend to distort into unreasonable geometries, so the general practice is to apply restraints on the bond distances and angles. With over 1.3 millions structures in the CSD, we have a pretty good ideal of normal values for bond distances and angles. A convenient way of establishing these averages is to do a Mogul geometry analysis, either natively or from within Mercury. I generally use the averages and standard deviations generated by Mogul as the restraints for my molecule.

Restraints are considered additional data in a Rietveld refinement, so we need to consider the relative weights of the raw data and the restraints. Most programs provide an easy way of adjusting the weights. I prefer to have the restraints contribute < 10% to the total χ^2 in the refinement, so that the refinement is nudged in the right direction by the restraints but is dominated by the data. Occasionally (for very large problems) the restraint weight needs to be higher, to keep the molecules together. Although torsion angles can be restrained, this is more complex, and since they are features in which I am interested, I do not restrain them. Planar groups (such as phenyl rings) can be restrained to be planar.

There is an additional feature to using restraints. You have to use the right values! I learned this the hard way, by making typographical errors when entering restraints. The refinement will duly adjust the molecule to the incorrect value, even with a low restraint weight. The restraints are somehow more important than we expect from their weights.

Similarly, it is uncommon to refine atomic displacement coefficients independently, although it sometimes possible to refine heavy atoms (such as S, Cl, Br, or I) anisotropically. More commonly, the U_{iso} are grouped by some form of chemical similarity, such as constraining all atoms in a ring system to have the same U_{iso}. It is uncommon to be able to refine hydrogen atoms, so I generally recalculate their positions (using molecular mechanics techniques) during the refinement, and fix their U_{iso} at some multiple (generally 1.2 or 1.3×) that of the displacement coefficient of the heavy atom to which they are attached.

Profile coefficients are important variables in a refinement. They affect the integrated intensities, which determine the structure. Most pharmaceutical patterns are dominated by microstrain broadening, so I tend to use such models to describe the peak profiles, especially the Stephens[11] anisotropic microstrain model. Microstrain tends to be Lorentzian, but sometimes one has to consider the Gaussian/Lorentzian mix in the pseudo-Voigt functions usually used to model peak profiles.

Preferred orientation is often a significant problem in laboratory flat plate specimens, especially if it is not obvious by inspection. Since it distorts the relative intensities of the peaks, it tends to compress electron density into planes or lines when trying to solve a

structure. Although preferred orientation can be modeled (as long as it is not too severe), it is always better to eliminate or minimize it by better specimen preparation. The capillary geometry commonly used at synchrotrons generally results in less preferred orientation, but sometimes it can be significant even in a rotated capillary specimen (Figure 7).

How do you measure the quality of a Rietveld refinement? Although there is no single measure, we can consider several classes[12]. The first are statistical measures. The most commonly used and useful are the weighted profile residual R_{wp} and the goodness-of-fit (GOF). Lower is better for both measures, but how low is low enough? The answer (as is the case for any question about powder diffraction) is "it depends".

The weighted profile residual is the weighted sum of the differences between observed and calculated data points divided by the weight sum of the observed intensities, and so contains the quantity minimized in the least squares. It is useful mainly as a relative indicator of better or poorer refinements. The absolute value depends on many things, such as the quality of the data (especially signal/noise), the quality/completeness of the model, the height of the background, and just about anything else one can imagine. With experience, you get a feel for what is good for your instrument of interest. To quantify, in Figure 8 are plotted the R_{wp} for > 130 pharmaceutical refinements I have done using synchrotron radiation. The median value is 8.6%, but the values range from < 1% to over 20%. All of these are what I consider correct structures! Just as with laboratory data, once R_{wp} gets below 10% you feel good about the quality of the fit.

The second common statistical measure is the goodness-of fit (GOF). This is the ratio between R_{wp} and the expected minimum residual calculated from the counting statistics. The ideal value is 1.00, which indicates that the residuals are dominated by statistical errors in the data, and not by any errors in the model. A value < 1 indicates that the weights are wrong, generally from a scaling of the raw data. The normal situation is GOF > 1, which indicates that there are systematic errors and/or the model is incomplete (or wrong). The simplest way to achieve a low GOF is to collect poor (noisy) data, but this is of course not what we want. Figure 9 reports the GOF values for my pharmaceutical synchrotron refinements. The average value is 1.5, so this is a reasonable expectation. Another measure of the quality fo the refinement is the ratio of the Rietveld R_{wp} to that obtained from a Le Bail or Pawley fit. If the ratio is < 2, the general rule of thumb is that the refinement is good.

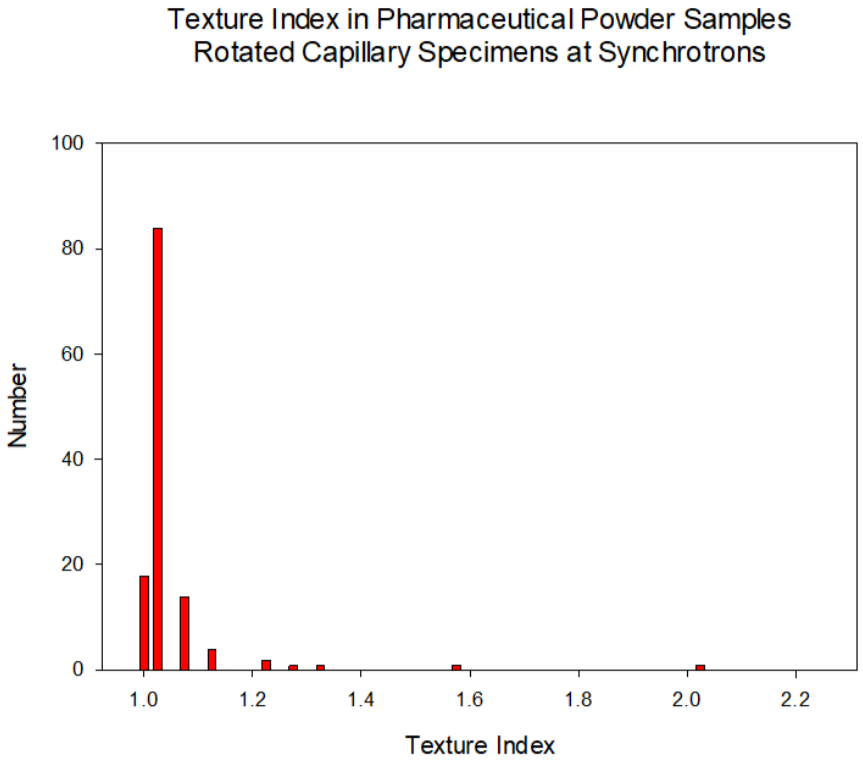

Figure 7. The texture index (indicating preferred orientation) in pharmaceutical structures determined by the author. A texture index = 1 indicates a random specimen, and a value of infinity indicates a single crystal.

Both of these distributions contain some larger-than-expected values. These tend to result from impurity peaks not included in the model, changes in peak shapes and/or positions resulting from change of the specimen during the measurement (beam damage), and incomplete modeling of the background, and the complexity of the problem (including potential disorder, which can be difficult to model using powder data). Sometimes you do the best you can, and move on to the next problem.

The second class of quality measures are graphical. Generally, in a structure paper there is one Rietveld plot, which contains observed, calculated, and difference intensities, sometimes with changes in intensity scale. This can be enough, but can hide information. In your own refinements, it is wise to do extensive zooming into small regions, to assess the nature of any mis-fits, and decide whether they can be corrected by changes to the model, or whether they have to be tolerated.

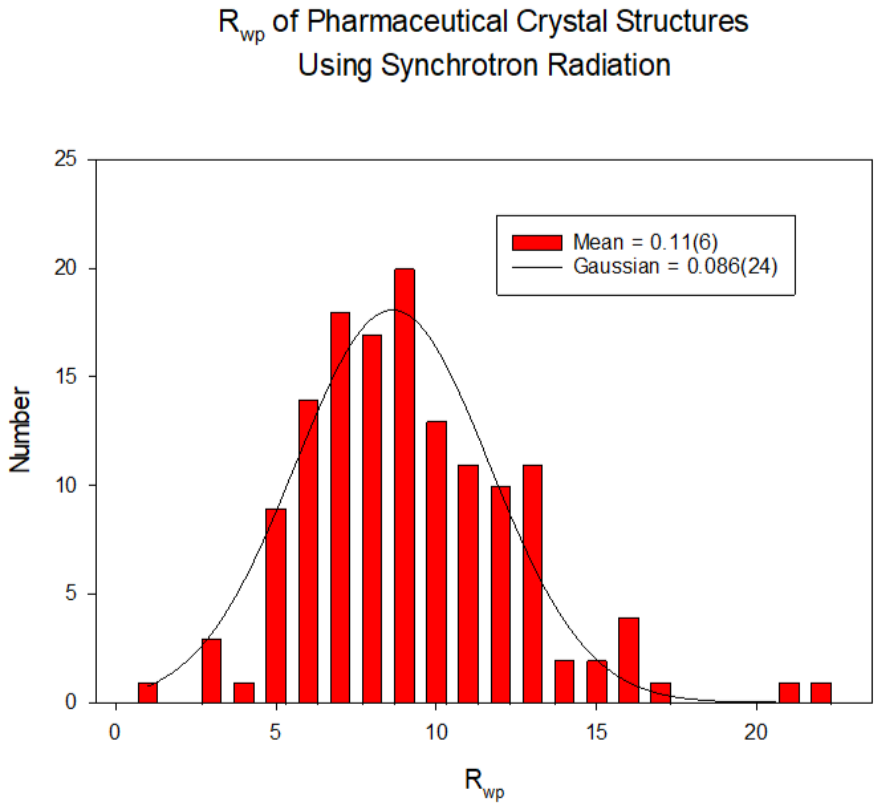

Figure 8. The weighted profile residual R_{wp} of a large number of pharmaceutical crystal structures determined by the author using synchrotron radiation.

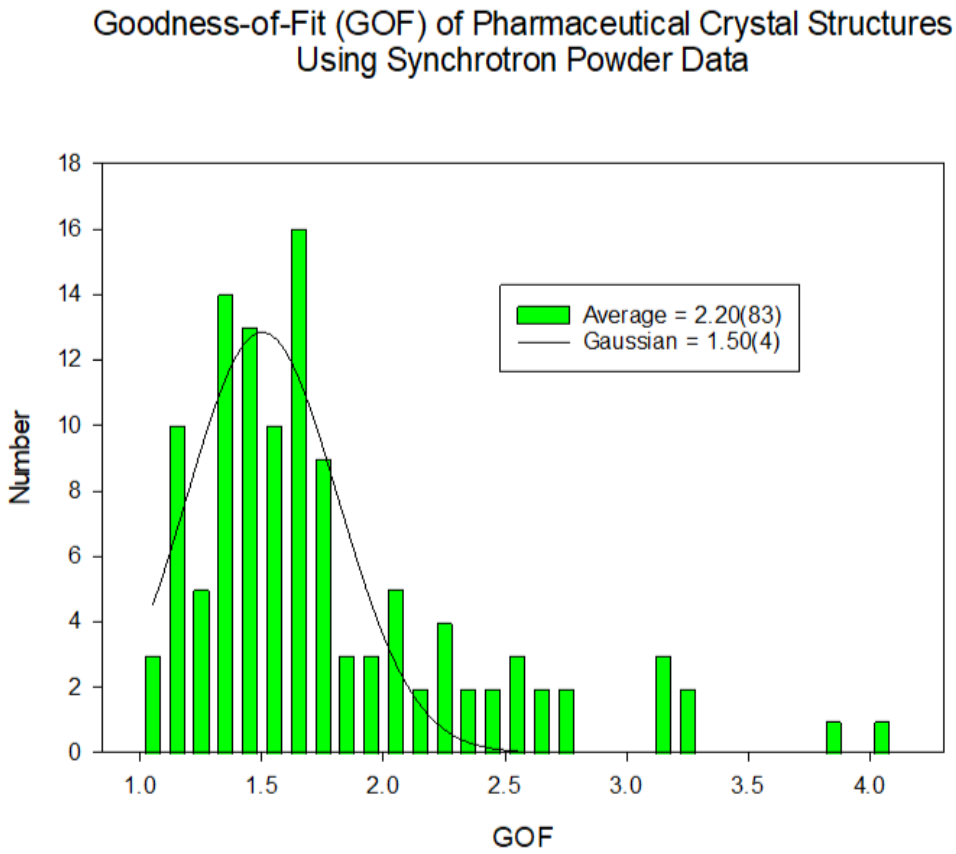

Figure 9. The Goodness-of-Fit values for a large number of pharmaceutical structures determined by the author using synchrotron radiation.

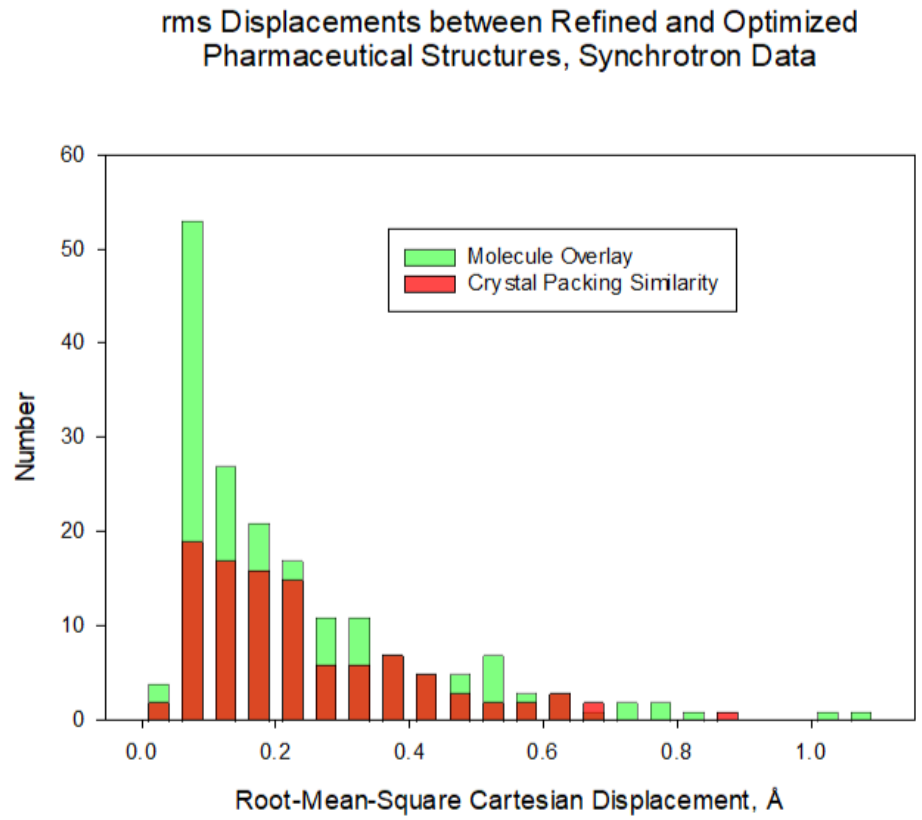

Figure 10. The root-mean-square Cartesian displacements between Rietveld-refined and DFT-optimized pharmaceutical crystal structures, determined using the Mercury Calculate Molecule Overlay tool (green) and the Crystal Packing Similarity tool (red).

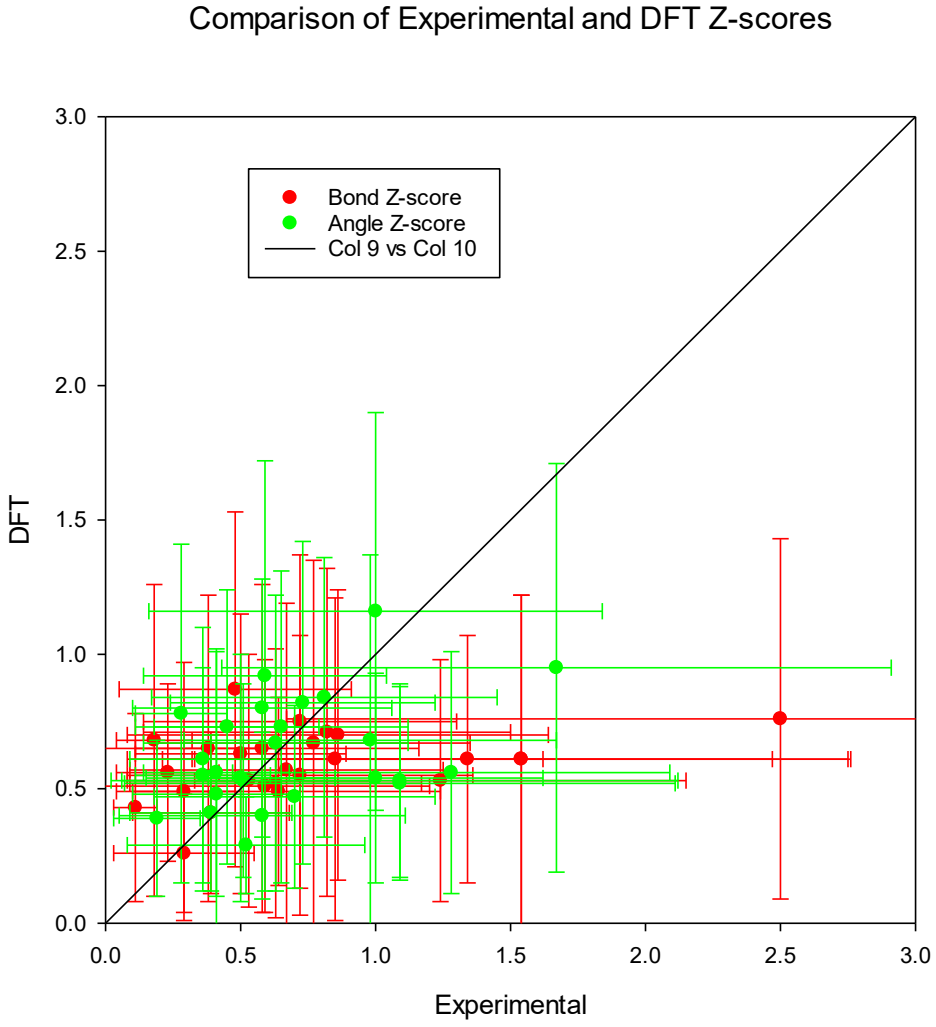

Figure 11. The average Z-score for bond distances (red) and bond angles (green) for experimental and DFT-optimized pharmaceutical crystal structures determined by the author.

Results

The third class of quality measures are what I like to call "chemical reasonableness"[12]. Again, there is no single quality measure, but we have to evaluate many different features of the structure.

The first thing to consider is the accuracy of the crystal structure. Quantifying the accuracy means knowing the correct answer. We don't know this from a single Rietveld refinement, but need additional information - perhaps spectroscopic and/or chemical and physical properties. Such information may not be available. One thing that has proven useful is to compare the refined structure to one optimized using density functional techniques.

Van de Streek and Neumann[13] compared over 200 refined single crystal structures with their DFT-optimized counterparts. The average root-mean-square Cartesian displacement between the pairs was 0.084 Å, and all were < 0.25 Å. Later they did a similar comparison for powder structures[14]. The average difference was 0.13 Å, and almost all were < 0.35 Å. In an overlay of two structures with an rms difference ~0.1 Å, the difference is hardly visible to the eye. We can consider such a DFT-optimized structure as essentially equivalent to a single-crystal structure, which is normally considered the gold standard for correctness.

Van de Streek and Neumann performed dispersion-corrected DFT optimizations and refined the lattice constants. Default DFT (without a dispersion model) tends to result in lattice parameters which are too large. I prefer to fix the lattice parameters at their experimental values, as we know them better than anything else in a Rietveld refinement. The authors of the DFT codes tell me that this is acceptable, and saves some computer time. Such geometry optimizations of pharmaceutical structures take days to weeks on a large local multiprocessor server, so are not trivial. Fixing the lattice parameters is acceptable if we are interested in the geometry. If the goal is to compare energies, then the lattice parameters should be refined in a dispersion-corrected DFT calculation.

Van de Streek et al.[15] have recently extended such comparisons, and suggest that the normal "crystallographic accuracy" is insufficient to obtain accurate values of energies and other physical and chemical properties, and suggest that we strive for "thermodynamic accuracy" in both refinements and optimizations. Small differences in atomic positions can have large effects on calculated properties. Among the examples is atorvastatin calcium trihydrate (Lipitor®), the structure of which had been solved using synchrotron powder data[16]. The structure agreed well with the experimental data, but two independent DFT optimizations disagreed with it and with each other. The structure was redetermined, and differences in the conformations of the flexible side chains of the two independent atorvastatin anions resulted. This new model agreed well with both the data and multiple DFT calculations. In considering energies, multiple DFT-D calculations are recommended to assess the accuracy of lattice energies.

Comparison of a Rietveld-refined structure and its DFT-optimized version is a good way of assessing the accuracy of the experimental structure. In (paid, with the CSD) Mercury, there are two convenient tools for making such comparisons. They are CSD-Materials/Search/Crystal Packing Similarity and Calculate/Molecule Overlay. The most appropriate may vary with the problem at hand. Distributions of such comparisons are presented in Figure 10. Although most fall within the range suggested by van de Streek and Neumann[14], some structures which I believe to be correct have larger disagreements. Reasons for this include the complexity of the structure, quality of the data (broad peaks and/or limited data range), preferred orientation, the presence of impurities, and/or incompletely modeled disorder. The way to avoid these large differences is probably to acquire/prepare a better sample.

Although DFT geometry optimizations on closed-shell systems such as most pharmaceuticals are generally quite reliable, there is some uncertainty associated with the results. Choices of program, basis sets, functionals, and control parameters may have small effects on the final geometry (and large effects on the energy). Occasionally chemically unreasonable results are obtained from a DFT calculation. Too-long S-N bonds in the DFT optimization of sulfonamides have been observed[17-19]. DFT programs have been shown to sometimes incorrectly locate hydrogen atoms, and miss the distinction between a salt and a co-crystal[20].

Another way to assess the accuracy of a crystal structure is to do a Mogul geometry analysis, and compare the structure to all of the others in the CSD. Each bond distance, bond angle, and torsion angle is compared to the similar ones in the CSD. A common metric is the "Z-score", the difference of the quantity of interest from the average value, divided by the standard uncertainty of the average. Perhaps surprisingly, the average Z-scores for most refined and optimized structures are similar (Figure 11), and < 1. In the refinements, the bond distances and angles were restrained to be near their average values, so the low Z-scores are to be expected. We would also expect that DFT optimization would yield chemically reasonable structures with distances and angles near the averages. The few structures with experimental Z-scores higher than the DFT ones indicate structures whose accuracy may not be as great as the others. These tend to be large refinements (160-210 least squares variables), and suggest that there are limits on the accuracy which can be expected from a powder structure.

A number of other factors can provide insight into the quality of the structure. Sometimes some displacement coefficients refine to larger-than-expected values, perhaps indicating disorder in a portion of the molecule. It can be difficult to model such disorder using powder data. An as-solved structure may contain voids, which may indicate the presence of unsuspected water/solvent molecules. A difference Fourier map can be instructive, even though such maps are flatter than single crystal maps. The "observed" structure factor amplitudes are biased by the structure model, so we expect such maps to be relatively flat. The largest peaks and holes in the

maps for most structures are < +/- 1.0 e/Å^3, or less than about 1 hydrogen atom. Sometimes a larger peak in a map will indicate the presence of a missing water/solvent molecule. If hydrogen bond donors and acceptors are present in the molecule, they almost always find each other in the crystal structure. If expected hydrogen bonds are not present, this can be a sign that the structure is incorrect. Examples are provided later.

The remaining discussion highlights and discusses (≤ 5 years) interesting and important structures, illustrating the applications of powder crystallography, major workers in the field, and journals in which the results are published.

Interest/Importance of Molecule/Structure

The chemically unreasonable structure of ibuprofen Form II, originally determined using powder data[21], was re-refined using the deposited raw data and combined with DFT optimization to yield an improved structure[22]. It was proposed that lack of a preferred orientation model in the initial refinement was the source of the problems in the original structure.

The structure of a new polymorph, β-L-tyrosine (prepared by sublimation), was determined using laboratory powder data[23]. It was difficult to index the pattern, because the sample contains a small concentration of the known α-polymorph. Once the unit cell was determined using 3D-ED, equivalent structures could be obtained independently using the X-ray powder and electron diffraction data sets. DFT optimization indicated that the new β-polymorph is metastable compared to the known α-polymorph.

The rhombohedral structure of a metastable Form II of oxcarbazepine (prepared by sublimation) was determined using laboratory powder data, assisted by crystal structure prediction[24]. The crystallites form by an unusual mechanism of condensed droplet formation and coalescence preceding nucleation and growth. The crystallites twist, limiting their size, and forcing determination using a powder sample.

The structure of a new metastable tetragonal form of the RNA polymerase inhibitor favipiravir was determined using laboratory powder data[25]. The hydrogen bond network differs from that in the stable orthorhombic polymorph, and there is no symmetry-allowed direct transformation path between the two polymorphs.

The structure of a co-crystal of remdesivir and salicylic acid was determined using laboratory powder data[26]. The structure solution and refinement were apparently straightforward, showing that synchrotron radiation is not strictly necessary.

The structure of Form I of the COVID-19 drug molnupirivir was solved using synchrotron powder data[27], virtually simultaneously with multiple single-crystal determinations.

Interesting Features of the Process

Although solving many structures using powder data is straightforward, issues can arise during the process of structure solution, which can make the process non-routine. Here are several examples from my own recent work (as I know more of the details) of the problems which can arise. I hope that knowing about these problems will help others in solving structures.

Indexing

The pattern of fluvoxamine maleate could not be indexed until up to 3 unindexed peaks were permitted. A $P2_1/c$ cell with a = 21.6310(15), b = 5.3180(4), c = 19.5555(15) Å, β = 99.979(5)°, V = 2215.48(25) Å^3 and Z = 4 was obtained, but this did not account for all of the peaks; there were several shoulders. All of the 2× supercells were examined, but these did not yield chemically reasonable solutions. The monoclinic cell yielded a reasonable solution. It is unclear whether the extra peaks resulted from beam damage[28].

Fruquintinib Form I crystallizes in space group C2 with a = 35.4167(22), b = 3.90500(12), c = 26.9370(11) Å, β = 108.0290(22)°, V = 3542.52(26) Å3, and Z = 8. Both the long and short axes made the pattern difficult to index, and a larger than normal number of peaks (31) had to be used for the indexing. Using the more-normal 20 peaks yielded smaller unit cells, which did not yield chemically reasonable structures[29].

The pattern of decoquinate was difficult to index[30]. The long 46 Å axis means that most of the low-angle peaks are of the form *h00* and *hk0*, and it was difficult to define the short axis. After several attempts (with smaller c-axes), the pattern was indexed on a primitive monoclinic unit cell with a = 46.77298, b = 12.95209, c = 7.65585 Å, β = 91.97°, V = 4635.24 Å^3, and Z = 8 (Z' = 2). For the structure solution (using MCSA techniques) the torsion angles of the decyl side chains were fixed at approximately 180°.

The pattern of anthraquinone-2-carboxylic acid was initially indexed on a $P2_1$ cell unit cell with a = 22.70667, b = 3.73900, c = 26.39351 Å, β = 106.563°, V = 2148.35 Å^3, and Z = 8 (Z' = 4), with up to 3 unindexed lines permitted. Structure solution and refinement were, however, unsatisfactory. The sample was recrystallized by sublimation (needle morphology) and the new pattern was indexed in *P-1* with a = 3.7942(2), b = 13.266(5), c = 22.835(15) Å, α = 73.355(30), β = 89.486(6), γ = 86.061(1)°, V = 1098.50(7) Å^3, and Z = 4 (Z' = 2). The structure was then successfully solved and refined in the correct space group[31].

The pattern of L-5-methyltetrahydrofolate calcium trihydrate could be indexed with difficulty in $P2_1$ with a = 6.9575, b = 6.5372, c = 53.7699 Å, β = 92.320°, V = 2444.33 Å^3, and Z = 4. Some plausible solutions were obtained, but they all contained some molecular overlap. Analysis of this cell using PLATON[32-33] showed that it was not the conventional monoclinic cell, which has a = 7.202, b = 6.548, c = 53.837 Å, and β = 90.54°. The fact that the β angle was close to 90° suggested exploration of orthorhombic unit cells. A better Le Bail fit was obtained in $P2_12_12_1$ with a = 7.1706(6), b = 6.5371(5), c = 53.8357(41) Å, V = 2523.58(26) Å^3, and Z = 4. In the best solution (by MCSA) the chirality of one of the C atoms was inverted, so had to be corrected manually[34].

Determination of Space Group

The pattern of cabotegravir could be indexed on a primitive orthorhombic unit cell with a = 31.4706(11), b = 13.4934(3), c = 8.43811(12) Å, V = 3583.201(18) Å^3, and Z = 8. A Le Bail fit in space group $P222$ accounted for all of the peaks, but the space group was ambiguous. Le Bail fits in six additional proper orthorhombic space groups ($P22_12_1$, $P2_122_1$, $P2_12_12$, $P2_122$, $P22_12$, and $P222_1$), as well as monoclinic space groups $P2_111$, $P12_11$, and $P112_1$ and the triclinic space group $P1$ were carried out. Space group $P22_12_1$ yielded a fit as good as $P1$, so it was adopted for structure solution[35], after converting the cell to the standard setting $P2_12_12$.

Delamanid crystallizes in space group $P2_12_12_1$ (#19) with a = 67.3701(18), b = 12.86400(9), c = 5.65187(12) Å, V = 4898.19(14) Å^3, and Z = 8. Establishing the space group was difficult. Several space group interpretation routines suggested the extinction symbol Pb_b, especially preferring $Pbnb$ (Z' = 1). The glide planes are inconsistent with pure R-delamanid. The highest ranked proper space group was $P2_12_12_1$, which would require Z' = 2. The structure was thus solved and refined in both $Pbnb$ and $P2_12_12_1$. The centrosymmetric space group (Pbnb) yielded Rwp ~20.4%, while the non-centrosymmetric space group (P$2_12_12_1$) yielded Rwp ~17.8% (with about twice as many parameters). To confirm the absence of a center of symmetry, a second harmonic test was carried out[36]. The SHG is a quadratic function of the laser power level, so the sample is non-centrosymmetric, and thus the suggested space group was $P2_12_12_1$.

The pattern of elvitegravir Form II was initially indexed on a primitive orthorhombic cell with a = 11.54903, b = 13.33241, c = 14.04233 Å, V = 2162.2 Å^3, and Z = 4. The space group was ambiguous, but P2_122_1 yielded an apparent successful solution and refinement of the structure. The structure solution contained a void on a 2-fold axis; the void was located in a reasonable position to form hydrogen bonds, so a water molecule was added to the model. A Rietveld refinement of 117 variables using 24,238 observations and 81 restraints yielded the residuals R_{wp} = 0.1399 and GOF = 2.14. The largest errors in the difference plot were in the intensities of many of the strong low-angle peaks, and the fit was overall disappointing. The root-mean-square Cartesian displacement between the Rietveld-refined and DFT-optimized structures was 0.341 Å, at the upper end of the normal range for correct structures. The unit cell did not account for the weak (0.6% relative intensity) 100 peak at 2.27°. While no one of these measures of the quality of the fit is necessarily a "red flag", their sum motivated concern about the correctness of the structure. Accordingly, the symmetry was lowered to P2_1 (to model the 100 peak), with a re-labeling of the axes to obtain the standard setting. This means that there are two molecules in the asymmetric unit, and thus that the problem was twice as large. The structure was re-solved in P2_1, and the success rate was only ~2%. TGA confirmed that the sample was anhydrous[37].

Chemical Reasonableness

It is common to deduce H atom positions (after MCSA using a neutral molecule) by analysis of potential hydrogen bonding, but sometimes the analysis is more complicated. It is almost always true that hydrogen bond donors and acceptors find each other in a crystal structure.

The pattern of reboxetine mesylate Form 2 was difficult to index, until a 3D ED structure of Form 1 appeared[38]. Once the Form 1 peaks could be identified, the pattern of Form 2 could be indexed on a monoclinic unit cell with Z' = 2. Two cations and two anions were used to solve the structure[39]. In the best solution, the protonated N in the morpholine ring of one molecule 1 formed the expected N-H···O hydrogen bonds to two anions, but the equivalent N in the other molecule did not. Examination of the structure showed that a C atom was 2.867 and 2.951 Å from two O atoms of the anions, and thus was probably a nitrogen atom. The atom types in this morpholine ring were reassigned manually and the hydrogen positions were recalculated using Mercury (conceptually rotating the ring by 180°) to obtain the model for refinement.

The best solution for palovarotene refined to Rwp = 0.0373, but was chemically unreasonable. There was a void, surrounded by hydrophilic groups (the carboxylic acid and pyrazole ring), but no hydrogen bonds. Visual examination of the structure revealed that, if both the pyrazole ring and the carboxylic acid group were rotated by ~180° the "free" N and hydroxyl group would become close enough to form an O-H···N hydrogen bond. Both the original and "flipped" structures were optimized using VASP (Kresse and Furthmüller, 1996). The "flipped" structure was 14.6 kcal/mol lower in energy than the original, so the final refinement was carried out using the flipped structure[40].

The cation in ractopamine hydrochloride contains two chiral centers, and commercial material is a mixture of four forms: S,S/R,R/S,R and R,S. Powder diffraction cannot distinguish between the pairs of enantiomers. Ractopamine hydrochloride crystallizes in space group $Pbca$ with a = 38.5871(49), b = 10.7691(3), c = 8.4003(2) Å, V = 3490.75(41) Å^3, and Z = 8. The (disordered) structure was solved and refined separately using the S,S and S,R diastereomers. The S,R form was significantly lower in energy[41].

Danofloxacin mesylate crystallizes in space group $P1$ with a = 6.77474(8), b = 12.4973(4), c = 12.82826(28) Å, α = 84.8709(29), β = 87.7501(10), γ = 74.9916(4)°, V = 1044.723(11) Å^3, and Z = 2 (Z' = 2). The structure was solved by Monte Carlo simulated annealing techniques, and the 11 best solutions were refined. In the two best solutions, the orientations of the cyclopropane rings and the methyl group on the diazobicycloheptane cages were the same. Each of the three N atoms in the cation is prochiral, so multiple sites for protonation had to be considered. The expected cation-anion N-H···O hydrogen bonds are not present, but there are cation-cation hydrogen bonds[42].

Meglumine diatrizoate crystallizes in space group $P2_1$ with a = 10.74697(4), b = 6.49364(2), c = 18.52774(7) Å, β = 90.2263(3), V = 1292.985(5) Å^3, and Z = 2. Two

different crystal structures, which yielded essentially identical refinement residuals and positions of the non-H atoms, were obtained. The differences were in the H atom positions and the hydrogen bonding. One structure was 123.0 kJ/mol/cell lower in energy than the other, and was adopted for the final description[43].

Butenafne hydrochloride crystallizes in space group $P2_1$ (#4) with a = 13.94806(5), b = 9.10722(2), c = 16.46676(6) Å, β = 93.9663(5)°, V = 2086.733(8) Å^3, and Z = 4 (Z' = 2). Although a reasonable initial refinement was obtained, the structure was chemically unsatisfactory. Only one of the cations formed the expected N-H···Cl hydrogen bond; the N···Cl distance was 3.061 Å. The corresponding N···Cl distance for the other cation was 3.619 Å. The butenafine free base molecule is achiral, but protonation can result in both *R* and *S* enantiomers. Both molecules were in the *R* configuration, as they were generated from two copies of a downloaded molecule. Manually inverting the configuration of the "long" cation from R to S performing a molecular mechanics-based structure optimization yielded the initial model for a much more satisfactory Rietveld refinement. Butenafine hydrochloride turns out to crystallize as a racemic co-crystal of enantiomers[44], explaining the Z' value of 2.

Difference in Chemistry

Benserazide hydrochloride Form I crystallizes in space group $P2_1/n$ (#14) with a = 19.22983(15), b = 14.45066(10), c = 4.57982(2) Å, β = 93.6935(3), V = 1270.014(15) Å^3, and Z = 4. The structure was solved by direct methods, but benserazide is a chiral molecule. What was purchased was an unintended racemate[45].

Lifitegrast sesquihydrate Form A crystallizes in space group $P2_1$ (#4) with a = 18.2526(4), b = 5.15219(6), c = 30.1962(6) Å, β = 90.8670(19), V = 2839.35(7) Å^3, and Z = 4. Thus, Z' = 2, and there are two lifetegrast molecules and two water molecules in the asymmetric unit of the presumed monohydrate. The structure was solved by Monte Carlo simulated annealing techniques and refined, and a moderate-sized void was noted. The void was large enough for a third water molecule, which would be stabilized by forming a number of hydrogen bonds. The compound is thus an unrecognized sesquihydrate[46].

Cariprazine hydrochloride (marketed as Vrayar) is used to treat a variety of psychological disorders. The structure of "cariprazine hydrochloride" was solved by direct methods, but an additional atom was located, and refined as a chloride ion. The compound purchased was thus cariprazine dihydrochloride[47]. Cariprazine dihydrochloride was also claimed in the patent[48], but no diffraction data was provided.

Large Structures

Structures with more than one molecule in the asymmetric unit ($Z' > 1$) are fairly common among pharmaceuticals. The presence of multiple fragments means that more variables are involved in both solution and refinement, and that the structure are automatically more challenging. Some notable recent examples are: quizartinib hydrate[49] and carbadox[50].

Accuracy

The crystal structure of nilotinib hydrochloride monohydrate was determined[51], and compared to the previously determined structure of the free base[52] and several solvates (single crystal structures). The accuracy of the synchrotron powder structure was high, and the precision (uncertainty) was only slightly worse than the single crystal structures. The cations in the hydrochloride and the free base molecule have very different conformations, so the comparison provides an opportunity to examine the detailed energetics of the system.

The crystal structure of doxorubicin was determined using laboratory powder data[53]. The assignment of the site of protonation was unambiguous. DFT optimization was used to confirm and analyze the structure. The rms Cartesian displacement between the Rietveld-refined and DFT-optimized structures was only 0.153 Å.

Salt/Cocrystal

As drug molecules get larger, their solubility tends to decrease. Salts and cocrystals of an API are often more soluble than the parent compound, increasing bioavailability, and are thus of great current interest. Many such structures are solved using powder data, especially when the materials are prepared using mechanochemical techniques.

As part of a virtual and experimental study of salts and co-crystals of riluzole and aromatic carboxylic acids[54], Voronin et al. isolated a new more-stable Form 2 of the salt of riluzole and 2,6-dihydroxybenzoic acid, and solved the structure using synchrotron powder data. The structure of Form 1 had been determined previously using single crystal data. The result permitted detailed comparison of the hydrogen bonding and energetics of the two forms. DFT calculations and the experiments clearly indicated that the two forms were salts, rather than co-crystals.

As part of a multicomponent solid form screening of ripretinib, the crystal structure of a ripretinib salt with ferulic acid was solved using high-resolution laboratory powder data[55]. The result clearly showed that the form was a salt. The hydrogen bonding was compared to that in a number of other salts and co-crystals determined using single crystal data.

A polymorph screening of raltegravir[56] yielded anhydrous Form A as well as two forms of a potential impurity C (methanol solvate). The structure of Form A and one of the Forms C were solved using laboratory powder data. Compared to the previously-determined K salt[57], the raltegravir molecule has a very different conformation; multiple sites for coordination to K in the salt affect the solid-state conformation. Not all of the hydrogen positions were located using the laboratory data.

The crystal structure of a 1:1 co-crystal of cephalexin and serine was solved and refined using laboratory powder data[58]. Both molecules are zwitterions, and the hydrogen bonding could be discussed in detail.

A computational method aimed at identifying

API/coformer pairs which are unlikely to form cocrystals was proposed[59]. This method can make experimental investigation of cocrystal formation more efficient. In the experimental portion of the study, the structures of cocrystals of carbamazepine and methylparabene and 2,4-t-butyl-4-methoxyphenol were determined using laboratory powder data. Synchrotron powder data was used to solve the structure of a cocrystal of carbamazepine and DL-tartaric acid, prepared by solvent-assisted grinding[60]. The structure of a carbamazepine:indomethacin cocrystal (as well as one of furosemide:urea) was solved using laboratory powder data[61]. Structures of several co-crystals of carbamazepine with dihydroxybenzoic acids were determined using laboratory powder data[62]. Knowledge of the structures facilitated quantitative phase analysis of mixtures obtained from mechanochemical reactions and determining the crystallization kinetics.

The structures of two forms of dexamethasone:resorcinol co-crystals were determined using laboratory powder data[63]. The molecular structure of dexamethasone in these cocrystals is virtually identical to that in pure dexamethasone[64]; the rms displacements are 0.066, 0.092, and 0.105 Å. Structures of co-crystals of dexamethasone with catechol and resorcinol were determined using laboratory powder data[65]. The co-crystals were more soluble than the parent dexamethasone.

The structures of a co-crystal of (*S*)-ibuprofen and L-proline and a quarter hydrate were determined using synchrotron powder data[66]. The structure solution was assisted by complementary techniques, including solid-state NMR, TGA, and dispersion-corrected DFT calculations. A powder study of the dehydration of the hydrate was also reported.

The crystal structure of a 1:1 co-crystal of creatine and citric acid was determined using laboratory powder data[67]. The creatine was a zwitterion and the citric acid as a neutral molecule.

The structure of a co-crystal of metaxolone and nicotinamide was determined using laboratory power data[68]. This co-crystal and other isostructural compounds had solubilities 3-9-fold higher than that of pure metaxolone.

A new 1:1 salt of the leprosy drug clofazimine and 4-aminobenzoic acid was prepared by liquid-assisted grinding, and the structure solved using laboratory powder data[69]. The salt is 5× more soluble than the free base.

The structure of a norfloxacin-nicotinic acid cocrystal, prepared by mechanochemical synthesis, was solved using laboratory powder data[70]. The cocrystal exhibited a pH-dependent solubility increases compared to pure norfloxacin.

Phase Transitions

Powder diffraction was used to characterize the phase transitions and desolvations in a series of solvates of nifedipine[71]. Most of the structures were solved from single crystals, but that of a low-temperature (100K) form of nifedipine:N,N-dimethylacetamide was solved directly from the *in situ* powder data. The molecular structure and hydrogen bonding could be analyzed in detail. This work emphasizes the importance of powder diffraction for *in situ* studies.

As part of an extensive experimental and computational study of polymorphism in the flexible molecule chlorpropamide, two solutions for η-chlorpropamide (prepared by mechanochemistry) were derived using powder data[72]. Crystal structure prediction was essential in sorting out the conformational landscape, but a larger energy range than typical must be considered when assessing metastable structures.

In a powder diffraction study of the formation of halobenzene (F, Cl, Br, and I) solvates of ibrutinib (the structures of which had been solved using single crystal techniques), an intermediate hemi(chlorobenzene) solvate was discovered, and its structure solved using the powder data[73]. The mechanism of solvate formation was investigated experimentally and computationally.

The crystal structures of Forms 1 and 4 of tafamidis were determined using laboratory powder data[74], and the details of the phase transitions were studied using in situ variable-temperature powder diffraction. The structure of Form I was determined independently using synchrotron powder data, and the details of the hydrogen bonding were characterized using DFT techniques[75].

Solid-state NMR information can reduce the search space of a structure prediction algorithm. The SSNMR data helped determine the correct tautomer and number of molecules in the asymmetric unit for mebendzole. The structures of phases A, B, and C were predicted correctly, and the structure of phase B was determined using powder data[76].

The structure of a new anhydrous Form III of bilastine and a chloroform/water mixed solvate were solved using synchrotron powder data[77]. Both this 1:1 solvate and a 3:1 chloroform:water solvate are transient phases, as they become unstable on removal from the mother liquor. Such unstable solvates can easily be overlooked in crystallization screenings.

Solution of the structures of multiple polymorphs of dantrolene and its hydrates, combined with single crystal studies of others, permitted rationalization of the reasons for polymorph formation[78]. The thermodynamic relationships among the polymorphs were established both experimentally and computationally.

The crystal structure of anhydrous mequitazine glycolate was determined using in situ laboratory powder data[79]. DFT-D calculations showed that hydrogen bonding by a bridging water molecule stabilized the hydrophilic layer of the hydrate more than that of the anhydrate. The structures of several cocrystals and hydrates of mequitazine were also solved using laboratory powder data[80].

At room temperature the anticancer drug carmustine was

amorphous, but at 153 and 278K the sample was crystalline, and the structure was determined using in situ laboratory powder data[81]. The molecules form a one-dimensional hydrogen bond pattern.

No additional polymorphs of lacosamide are obtained on heating from room temperature, but two additional low-temperature polymorphs were discovered[82]. The structure of one of these was solved using laboratory powder data. The structures are distinct, but similar, and the phase transformations are completely reversible.

Synchrotron powder data was used to solve the structure of a new intermediate anhydrous form of ciprofloxacin hydrochloride, prepared by heating the commercial hydrate[83]. Both structures contain 1D chains and 2D sheets. The structure of a ciprofloxacin:thymol cocrystal was solved using laboratory powder data[84].

The structures of several polymorphs of sofosbuvir, prepared by liquid-assisted grinding, were solved using laboratory powder data[85]. Transformation to the most stable form can occur through different intermediate forms.

Future Outlook

Recent advances in structure prediction[86-87] may lessen the need to solve structures *ab initio* from powder data. The results of a structure prediction generally consist of a library of potential low-energy structures. Comparing the calculated powder patterns of such structures to experimental data should enable choice of the correct structure. It may even be possible to establish the structures of the components of mixtures.

Although small numbers (10-20/year) of drug structures have been solved using electron diffraction techniques[88], recent advances in 3DED/Micro-ED instruments and techniques[38] may also lessen the need for *ab initio* structure solution using powder data. Essentially single crystal data sets are collected on the individual crystallites in a powder sample. It may be easier to solve a structure using such single crystal data, but a better structure refinement may be obtained by the Rietveld method using X-ray powder data. Certainly, the powder refinement will yield more-precise lattice parameters, and thus more-precise geometrical parameters. It remains to be seen how prevalent damage to the pharmaceutical sample in the electron beam will be. Powder diffraction will always have a role in *in situ* studies and in characterization of formulated products.

References

1. Zagorac D, Müller H, Ruehl S, Zagorac J, Rehme S. 2019. Recent developments in the Inorganic Crystal Structure Database: theoretical crystal structure data and related features. Journal of Applied Crystallography. 2019; 52: 918-925.
2. Groom CR, Bruno IJ, Lightfoot MP, Ward, SC. The Cambridge Structural Database. Acta Crystallographica Section B: Structural Science, Crystal Engineering and Materials. 2016; 72: 171-179.
3. Boldyreva EV, Ivashevskaya SN, Sowa H, Ahsbahs H, Weber H-P. Effect of hydrostatic pressure on the γ-polymorph of glycine. 1. A polymorphic transition into a new δ-form. Z. Krist. Cryst. Mater. 2005; 220: 50-57.
4. Kabekkodu S, Dosen A, Blanton TN. PDF-5+: a comprehensive powder diffraction file™ for materials characterization. Powder Diffraction 2004; 39: 47-59.
5. Madsen, I C, Scarlett NVY, Kleeberg R, Knorr K. 2019. Quantitative phase analysis. 2019. Chapter 3.9 in *International Tables for Crystallography Volume H: Powder Diffraction*, 344-373.
6. Baerlocher C, McCusker LB. 2002. The structure determination process. 2002. in Structure Determination from Powder Diffraction Data, edited by David WIF, Shankland K, McCusker LB, Baerlocher C, 4-7.
7. David WIF. 2019. Real-space methods for structure solution frm powder-diffraction data: application to molecular structures. 2019. Chapter 4.3 in *International Tables for Crystallography Volume H: Powder Diffraction*, 414-432.
8. USP. Characterization of Crystalline and Partially-Crystalline Solids by X-ray Powder Diffraction (XRPD). 2022. Section 941.
9. Le Bail A. 2019. Data reduction to $|F_{hkl}|$ values. 2019. Chapter 3.5 in *International Tables for Crystallography Volume H: Powder Diffraction*, 282-287.
10. Rizzi R, Palatinus L, Kaduk JA. 2025. Crystal Structure Determination. , 2025. Chapter 8 in R. E. Dinnebier and S. J. L. Billinge, *Powder Diffraction: Theory and Practice*, 2nd edition.
11. Stephens PW. Phenomenological Model of Anisotropic Peak Broadening in Powder Diffraction. Journal of Applied Crystallography 1999; 32: 281-289.
12. Kaduk JA. 2019. Structure validation. 2019; Chapter 4.9 in *International Tables for Crystallography Volume H: Powder Diffraction*, 489-514.
13. van de Streek J, Neumann M. Validation of experimental molecular crystal structures with dispersion-corrected density functional theory calculations. Acta Crystallographica Section B 2010; 66: 544-558.
14. van de Streek J, Neumann M. Validation of moleculr crystal structures from powder diffraction data with dispersion-corrected density functional theory (DFT-D). Acta Crystallographica Section B 2014; 70: 1020-1032.
15. van de Streek J, Firaha D, Kaduk JA, Blanton TN. From 'crystallographic accuracy' to 'thermodynamic accuracy': a redetermination of the crystal structure of calcium atorvastatin trihydrate (Lipitor®). Acta Crystallographica Section B 2024; 80: 682-687.
16. Hodge RL, Kaduk JA, Gindhart AM, Blanton TN. Crystal structure of atorvastatin calcium trihydrate Form I (Lipitor®), $(C_{33}H_{34}FN_2O_5)_2Ca(H_2O)_3$. Powder Diffraction 2020; 35: 136-143.
17. Kaduk JA, Dosen A, Blanton TN. Crystal structure of aprocitentan Form A, $C_{16}H_{14}Br_2N_6O_4S$. submitted to Powder Diffraction 2025.
18. Vibha K, Prachality NC, Reddy RA, Ravikantha MN, Thipperudrappa J. Computational studies on sulfonamide drug molecules by density functional theory. Chemical Physics Impact 2023; 6: 100147.
19. Whitfield PS. Structure Solution of Sulphonamides from Powder Diffraction Data - A Problematic Moiety? presented at the 18th Pharmaceutical Powder X-ray Diffraction Symposium, Cambridge UK, 8 May 2025.
20. Chalupná SM, Hušák M, Čejka J, Fňukal F, Klimeš J. Computation screening for incorrectly determined cocrystal structures. Acta Crystallographica Section B: Structural Science Crystal Engineering Materials 2025; 81: 208-216.
21. Derollez PE, Dudognon F, Affouard F, Danede F, Correia NT, Descamps M. Ab initio Structure Determination of Phase II of Racemic Ibuprofen by X-ray Powder Diffraction. Acta Crystallographica 2010; B66: 76-80; CSD Refcode IBPRAC04.
22. Whitfield PS, Smalley CJ. A Critical Examination and Re-Determination of the Literature Ibuprofen Form-II Structure. Advances in X-ray Analysis2022; 66: 85-94; CSD Refcode IBPRAC24.
23. Smalley CJS, Hoskins HE, Hughes CE, Johnstone DN, Willhammar T, Young MT, Pickard CJ, Logsdail AJ, Midgley PA, Harris KDM. A structure determination protocol based on combined analysis of 3D-ED data, powder XRD data, solid-state NMR data and DFTD calculations reveals the structure of a new polymorph of L-tyrosine. Chemical Science 2022; 13: 5277-5288; CSD Refcode LTYROS14.
24. Polyzois H, Guo R, Srirambhatla VK, Warzecha M, Prasad E, Turner A, Halbert GW, Keating P, Price SL, Florence AJ. Crystal Structure and Twisted Aggregates of Oxcarbazepine Form III. Crystal Growth & Design 2022; 22: 4146-4156; CSD Refcode CANDUR03.
25. Goloveshkin AS, Korlyukov AA, Vologzhanina AV. Novel Polymorph of Favipiravir - An Antiviral Medication. Pharmaceuticals2021; 13: 139.
26. Wong SN, Low K-H, Poon YL, Zhang X, Chan HW, Chow SF. Synthesis of the first remdesivir cocrysal: design, characterization, and therapeutic potential for pulmonary delivery. International Journal of Pharmaceutics 2023; 640: 122983; CSD Refcode ZILNAN.
27. Ens TM, Kaduk JA, Rost MM, Dosen A, Blanton TN. Hydrogen bonding in the crystal structure of molnupiravir Form I, $C_{13}H_{19}N_3O_7$. Powder Diffraction 2025; 40: 72-75.
28. Kaduk JA, Dosen A, Blanton TN. Crystal structure of fluvoxamine maleate, $(C_{15}H_{22}F_3N_2O_2)(HC_4H_2O_4)$. submitted to Powder Diffraction 2025.
29. Kaduk JA, Dosen A, Blanton TN. A proposed crystal structure of fruquintinib Form I, $C_{21}H_{19}N_3O_5$. submitted to Powder Diffraction 2025.
30. Ens TM, Kaduk JA, Rost MM, Dosen A, Blanton TN.

Crystal structure of decoquinate, $C_{24}H_{35}NO_5$. Powder Diffraction 2025; 40(1); 57-64.
31. Ens TM, Kaduk JA, Dosen A, Blanton TN. Crystal structure of anthraquinone-2-carboxylic acid, $C_{15}H_8O_4$. Powder Diffraction 2024; 39: 29-35.
32. Spek AL. Structure Validation in Chemical Crystallography. Acta Crystallographica 2009; D 65: 148-155.
33. Spek AL. CheckCIF Validation Alerts: What They Mean and How To Respond. Acta Crystallographica E 2020; 76: 1-11.
34. Kaduk JA, Patel NV, Golab JT. Crystal structure of calcium L-5-methyltetrahydrofolate trihydrate Type I, $C_{20}H_{23}N_7O_6Ca(H_2O)_3$. Powder Diffraction 2023; 38: 207-214.
35. Kaduk JA, Dosen A, Blanton TN. Proposed crystal structure of cabotegravir, $C_{19}H_{17}F_2N_3O_5$. submitted to Powder Diffraction 2025.
36. Ens TM, Kaduk JA, Rost MM, Dosen A, Blanton TN. A proposed crystal structure of delamanid, $C_{25}H_{25}F_3N_4O_6$. submitted to Powder Diffraction 2025.
37. Kaduk JA, Gates-Rector S, Blanton TN. Crystal structure of elvitegravir Form II, $C_{23}H_{23}ClFNO_5(H_2O)_{0.27}$. Powder Diffraction 2023; 38: 53-63.
38. Lin J, Bu G, Unge J, Gonen T. Uncovering the Elusive Structures and Mechanisms of Prevalent Antidepressants. BioRchiv preprint https://doi.org/10.1101/2024.01.04.574264, posted 5 January 2024.
39. Kaduk JA, Dosen A, Blanton TN. Crystal structure of Form 2 of racemic reboxetine mesylate, $(C_{19}H_{24}NO_3)(CH_3O_3S)$. submitted to Powder Diffraction 2025.
40. Kaduk JA, Dosen A, Blanton TN. Crystal structure of palovarotene, $C_{27}H_{30}N_2O_2$. submitted to Powder Diffraction 2025.
41. Scherry CW, Boaz NC, Kaduk JA, Dosen A, Blanton TN. Crystal structure of ractopamine hydrochloride, $C_{18}H_{14}NO_3Cl$. Powder Diffraction 2024; 39: 94-104.
42. Ens TM, Kaduk JA, Dosen A, Blanton TN. Crystal structure of danofloxacin mesylate, $(C_{19}H_{21}FN_3O_3)(CH_3O_3S)$. Powder Diffraction 2023; 38: 194-200.
43. Ens TM, Kaduk JA, Dosen A, Blanton TN. Crystal structure of meglumine diatrizoate, $(C_7H_{18}NO_5)(C_{11}H_8I_3N_2O_4)$. Powder Diffraction 2023; 38: 185-193.
44. Kaduk JA, Gates-Rector S, Blanton TN. Crystal structure of butenafine hydrochloride, $C_{23}H_{28}NCl$. Powder Diffraction 2023; 38: 30-36.
45. Kaduk JA, Dosen A, Blanton TN. Crystal structure of benserazide hydrochloride form I, $C_{10}H_{16}N_3O_5Cl$. Powder Diffraction 2025; 40: 65-71.
46. Kaduk JA, Rost MM, Dosen A, Blanton TN. Proposed crystal structure of lifitegrast sesquihydrate Form A, $(C_{29}H_{24}Cl_2N_2O_7S)_2(H_2O)_3$. Powder Diffraction 2024; 39: 275-282.
47. Kaduk JA, Rost MM, Dosen A, Blanton TN. Crystal structure of cariprazine dihydrochloride, $C_{21}H_{34}Cl_2N_4OCl_2$. Powder Diffraction 2025; 40: 89-93.
48. Czibula L, Sebok F, Greiner I, Domany G, Csongor EA. Salts of piperazine compounds as D_3/D_2 antagonists. United States Patent 2011; 7,943,621 B2.
49. Kaduk JA, Dosen A, Blanton TN. Crystal structure of quizartinib hydrate, $C_{29}H_{32}N_6O_4S(H_2O)_{1/3}$. submitted to Powder Diffraction 2025.
50. Kaduk JA, Dosen A, Blanton TN. Proposed crystal structure of carbadox, $C_{11}H_{20}N_3O_3$. Powder Diffraction 2024; 39: 82-93.
51. Goloveshkin AS, Kulikova ES, Novikov RA, Vologzhanina AV, Korlyukov AA. Crystal structure of nilotinib hydrochloride monohydrate according to powder X-ray diffraction data. Journal of Structural Chemistry 2024; 65: 585-595; CSD Refcode KOQNAJ.
52. Kaduk JA, Zhong K, Gindhart AM, Blanton TN. Crystal structure of nilotinib, $C_{28}H_{22}F_3N_7O$. Powder Diffraction 2015; 30: 270-277.
53. Bezzon VDN, Dos Santos Caturello NAM, Dalpian GM, Ferreira FF. Crystal structure determination and DFT analysis of doxorubicin hydrochloride for controlled-release drug formulations. Journal of Molecular Structure 2023; 1294: 136412; CSD Refcode RIPJAF.
54. Voronin AP, Ramazanova AG, Churakov AV, Vologzhanina AV, Kulikova ES, Perlovich GL. Virtual Screening, Polymorphism, and Formation Thermodynamics Study of Riluzole Multicomponent Crystals with Dihydroxybenzoic Acids. Crystal Growth & Design 2024; 24: 9773-9789; CSD Refcode KUKHIL01.
55. Muthaiyan M, Fayaz FTS, Kenguva G, Prajapati AK, Dandela R, Chernyshev VV, Sanphui P. "New Multicomponent Solid Forms of the Antitumor Drug Ripretinib: The Role of Conformations in Dictating Dissolution and Photostability. Crystal Growth & Design 2024; 24: 7617-7631; CSD Refcode HOXMEQ.
56. Fayaz TKS, Chanduluru HK, Lal P, Ghosh A, Chernyshev V, Sanphui P. Structural analysis of anti-retroviral drug raltegravir and its potential impurity C: investigation of solubility and stability. CrystEngComm 2024; 26: 517-531; CSD Refcode DOKNEA.
57. Kaduk JA, Zhong K, Gindhart AM, Blanton TN. Crystal structure of raltegravir potassium, $C_{20}H_{20}FKN_6O_6$. Powder Diffraction 2015; 30: 263-269; CSD Refcode URAVIU.
58. Fayaz TKS, Palanisamy V, Sanphui P, Chernyshev V. Multicomponent solid forms of antibiotic cephalexin towards improved chemical stability. CrystEngComm 2023; 25: 1252-1262; CSD Refcode TEXRAT.
59. Sugden IJ, Braun DE, Bowskill DH, Adjiman CS, Pantelides CC. Efficient Screening of Coformers for Active Pharmaceutical Ingredient Cocrystallization. Crystal Growth & Design 2022; 22: 4513-4527; CSD Refcodes HEDYAU, HEDYIC, and HEDYIC01.
60. Guerain M, Derollez P, Roca-Paixão L, Dejoie C, Correia NT, Afouard F. Structure determination of a new cocrystal of carbamazepine and DL-tartaric acid by synchrotron powder X-ray diffraction. Acta Crystallographica Section C: Structural Chemistry 2020; 76: 225-230.
61. Al Rahal O, Majumder M, Spillman MJ, van de Streek J, Shankland K. Co-Crystal Structures of Furosemide:Urea and Carbamazepine:Indomethacin Determined from Powder X-ray Diffraction Data. crystals 2020; 10: 42.
62. Martins ICB, Emmerling F. Carbamazepine Dihydroxybenzoic Acid Cocrystals: Exploring Packing

Interactions and Reaction Kinetics. Crystal Growth & Design 2021; 21: 6981-6970.
63. Wong SN, Low K-H, Weng J, Chan HW, Chow SF. Expanding the solid-state landscape of dexamethasone: a specific sandwich structure in facilitating the formation of kinetically stable cocrystals from mechanochemistry. CrystEngComm 2022; 24: 5875-5879; CSD Refcode BEGKUX.
64. Raynor JW, Minor W, Chruszcz M. Dexamethasone at 119K. Acta Crystallographica Section E: Structure Reports Online 2007; 63: o2791-02793; CSD Refcode DEXMET11.
65. Varsa RB, Sanphui P, Chernyshev V. Polymorphs and isostructural cocrystals of dexamethasone: towards the improvement of aqueous solubility. CrystEngComm 2022; 24: 6045-6058; CSD Refcodes GEGKUX01 and HAYBAO01.
66. Al Rahal O, Williams PA, Hughes CE, Kariuki BM, Harris KDM. Structure Determination of Multicomponent Crystalline Phases of (S)-Ibuprofen and L-Proline from Powder X-ray Diffraction Data, Augmented by Complementary Experimental and Computational Techniques. Crystal Growth & Design 221; 21: 2498-2507.
67. Pekar KB, Lefton JB, McConville CA, Burleson J, Sethio D, Kraka E, Runčevski T. Mechanosynthesis of a Coamorphous Formulation of Creatine with Citric Acid and Humidity-Mediated Transformation into a Cocrystal. Crystal Growth & Design 2021; 21: 1297-1306.
68. Gohel SK, Palanisamy V, Sanphui P, Prakash M, Singh GP, Chernyshev V. Isostructural cocrystals of metaxolone with improved dissolution characteristics. RSC Advances 2021; 11: 30689-30700.
69. Sousa ML, Sarraguça MC, Oliveira dos Santos A, Sarraguça JMG, Lopes J, Ribeiro PRS. A new salt of clofazimine to improve leprosy treatment. Journal of Molecular Structure2020; 1214: 128226.
70. Ferreira PO, Cosmo de Almeida A, Carvalho dos Santos E, Droppa Junior R, Ferreira FF, Kogawa AC, Caires FJ. A norfloxacin-nicotinic acis cocrystal: Mechanochemical syntheses, thermal and structure characterization and solubility assays. Thermochimica Acta 2020; 694: 178782.
71. Jones ECL, Goldsmith KE, Ward MR, Bimbo LM, Oswald IDH. Exploring the thermal behaviour of the solvated structures of nifedipine. 2023. Acta Crystallographica Section B: Structural Science, Crystal Engineering, and Materials 2023; 79: 164-175; CSD Refcode HEZWES.
72. Ward MR, Taylor CR, Mulvee MT, Lampronti GI, Belebguer AM, Steed JW, Day GM, Oswald IDH. Pushing Technique Boundaries to Probe Conformational Polymorphism. Crystal Growth & Design 2023; 23: 7217-7230; CSD Refcodes BEDMIG20 and BEDMIG21.
73. Jirát J, Rohlíček J, Kaminsky J, Jirkal T, Ridvan L, Skořepová E, Zvoníček V, Dušek M, Šoóš M. Formation of ibrutinib solvates: so similar, yet so different. IUCrJ 2023; 10: 210-219.
74. Masciocchi N, Abbinate VM, Zambra M, Barreca G, Zampieri M. Thermal and Structural Characterization of Two Crystalline Polymorphs of Tafamidis Free Acid. Molecules 2022; 27: 7411; CSDRefcodes CEGDOV and CEQDOV01.
75. Ens TM, Kaduk JA, Dosen A, Blanton TN. Powder X-ray diffraction of tafamidis Form 1, $C_{14}H_7Cl_2NO_3$. Submitted to Powder Diffraction 2025.
76. Bravetti F, Bordignon S, Alig E, Eisenbeil D, Fink L, Nervi C, Gobetto R, Schmidt MU, Chierotti MR. Solid-State NMR-Driven Crystal Structure Prediction of Molecular Crystals: The Case of Mebendazole. Chemistry - A European Journal 2022; 28: e202103589; CSD Refcode SIYTED.
77. Puigjanaer C, Portell A, Blasco A, Font-Bardia M, Vallcorba O. Entrapped Transient Chloroform Solvates of Bilastine. crystals 2021; 11: 342.
78. Kons A, Mishnev A, Mukhametzyanov TA, Buzyurov AV, Lapuk SE, Berzins A. Hexamorphism of Dantrolene: Insights into the Crystal Structures, Stability, and Phase Transformations. Crystal Growth & Design 2021; 21: 1190-1201.
79. Okura R, Uchiyama H, Kadota K, Tozuka Y. Hydrogen bonding fro crystalline water mediates the hydration/dehydration of mequitazine glycolate. CrystEngComm 2021; 23: 4816-4824.
80. Okura R, Uchiyama H, Kadota K, Tozuka Y. New Salt and Cocrystal of Mequitazine: Impact of Coformer Flexibility and Hydrogen Bond Donors on Polymorphism. Crystal Growth & Design 2020; 20: 7219-7229.
81. Schlessinger C, Alig E, Schmidt MU. Crystal structure of the anticancer drug carmustine determined by X-ray powder diffraction. Powder Diffraction 2021; 36: 148-150.
82. Skořepová E, Rohlíček J, Chatziadi A, Zvoníček V, Jirát J, Čejka J, Ridvan L, Šoóš M. Low-temperature polymorphs of lacosamide. Journal of Crystal Growth 2021; 562: 126085.
83. Putra OD, Pettersen A, Yonemochi E, Uekusa H. Structural origin of physicochemical properties differences upon dehydration and polymorphic transformation of ciprofloxacin hydrochloride revealed by structure determination from powder X-ray diffraction data. CrystEngComm 2020; 22: 7272-7279.
84. Shemchuk O, D'Agostino S, Fiore C, Sambri V, Zannoli S, Grepioni F, Braga D. Natural Antimicrobials Meet a Synthetic Antibiotic: Carvacrol/Thymol and Ciprofloxacin Cocrystals as a Promising Solid-State Route to Activity Enhancement. Crystal Growth & Design 2020; 20: 6796-6803.
85. Chatziadi A, Skořepová E, Rohlíček J, Dušek M, Ridvan L, Šoóš M. Mechanochemically Induced Polymorphic Transformations of Sofosbuvir. Crystal Growth & Design 2020; 20: 139-147.
86. Hunnisett LM, Nyman J, Francia N, Abraham NS, Adjiman CS, Aitipamula S, Alkhidir T, Almehairbi M, Anelli A, Anstine DM, Anthony JE, Arnold JE, Bahrami F, Bellucci MA, Bhardwaj RM, Bier I, Bis JA, Boese AD, Bowskill DH, Bramley J, Brandenburg JG, Braun DE, Butler PWV, Cadden J, Carino S, Chan EJ, Chang C, Cheng B, Clarke SM, Coles SJ, Cooper RI, Couch R, Cuadrado R, Darden T, Day GM, Dietrich H, Ding Y, DiPasquale A, Dhokale B, Van Eijck BP, Elesgood MRJ, Firaha D, Fu W, Fukuzawa K, Glover J, Goto H, Greenwell C, Guo R, Harter J, Hellferich J, Hofmann DWM, Hoja J, Hone J, Hong R, Hutchison G, Ikabata Y, Isayev O, Ishaque O, Jain V, Jin Y, Jing A, Johnson ER, Jones I, Jovan Jose KV, Kabova EA, Keates A,

Khakimov D, Konstantinopoulos S, Kuleshova LN, Li H, Lin X, List A, Liu C, Liu YM, Liu Z, Liu Z-P, Lubach JW, Marom N, Maryewski AA, Matsui H, Mattei A, Mayo RA, Melkumov JW, Moamed S, Abardeh ZM, Muddana HS, Nakayama N, Nayal KS, Neumann MA, Nikhar R, Obata S, O'Connor D, Organov AR, Okuwaki K, Otero-de-la-Roza A, Pantelides CC, Parkin S, Pickard CJ, Pilia L, Pivina T, Podeszwa R, Price AJA, Price LS, Price SL, Probert MR, Pulido A, Ramteke GR, Rehman AU, Reutzel-Edens SM, Rogal J, Ross AJ, Rumson AF, Sadiq G, Saeed ZM, Salimi A, Salvalaglio M, Sanders de Almada L, Sasikumar K, Sekharan S, Shang C, Shankland K, Shinohara K, Shi B, Shi X, Skillman AG, Song H, Strasser N, van de Streek J, Sugden IJ, Sun G, Szalewicz K, Tan BI, Tan L, Tarczynski F, Taylor CR, Tkatchenko A, Tom R, Tuckerman ME, Utsumi Y, Vogt-Maranto L, Weatherston J, Wilkinson LJ, Willacy RD, Wojtas L, Woollam GR, Yang Z, Yonemochi E, Yue X, Zeng Q, Zhang Y, Zhou T, Zhou Y, Zubatyuk R, Cole JC. The seventh blind test of crystal structure prediction: structure generation methods. Acta Crystallographica Section B: Structural Science Crystal Engineering Materials 2024; 80: 517-547.

87. Hunnisett LM, Francia N, Nyman J, Abraham NS, Aitipamula S, Alkhidir T, Almehairbi M, Anelli A, Anstine DM, Anthony JE, Arnold JE, Bahrami F, Bellucci MA, Beram GJO, Bhardwaj RM, Bianco R, Bis JA, Boese AD, Bramley J, Braun DE, Butler PWV, Cadden J, Carino S, Červinka C, Chan EJ, Chang C, Clarke SM, Coles SJ, Cook CJ, Cooper RI, Darden T, Day GM, Deng W, Dietrich H, DiPasquale A, Dhokale B, Van Eijck BP, Elesgood MRJ, Firaha D, FuW, Fukuzawa K, Galanakis N, Goto H, Greenwell C, Guo R, Harter J, Hellferich J, Hoja J, Hone J, Hong R, Hušák M, Ikabata Y, Isayev O, Ishaque O, Jain V, Jin Y, Jing A, Johnson ER, Jones I, Jovan Jose KV, Kabova EA, Keates A, Kelly PF, Klimeš J, Kostkova V, Li H, Lin X, List A, Liu C, Liu YM, Liu Z, Lončarič I, Lubach JW, Ludik J, Marom N, Matsui H, Mattei A, Mayo RA, Melkumov JW, Mladineo B, Moamed S, Abardeh ZM, Muddana HS, Nakayama N, Nayal KS, Neumann MA, Nikhar R, Obata S, O'Connor D, Organov AR, Okuwaki K, Otero-de-la-Roza A, Parkin S, Parunov A, Podeszwa R, Price AJA, Price LS, Price SL, Probert MR, Pulido A, Ramteke GR, Rehman AU, Reutzel-Edens SM, Rogal J, Ross AJ, Rumson AF, Sadiq G, Saeed ZM, Salimi A, Sasikumar K, Sekharan S, Shankland K, Shi B, Shi X, Shinohara K, Skillman AG, Song H, Strasser N, van de Streek J, Sugden IJ, Sun G, Szalewicz K, Tan L, Tang K, Tarczynski F, Taylor CR, Tkatchenko A, Tom R, Touš P, Tuckerman ME, Unuzeta PA, Utsumi Y, Vogt-Maranto L, Weatherston J, Wilkinson LJ, Willacy RD, Wojtas L, Woollam GR, Yang Y, Yang Z, Yonemochi E, Yue X, Zeng Q, Zhou T, Zhou Y, Zubatyuk R, Cole JC. The seventh blind test of crystal structure prediction: structure ranking methods. Acta Crystallographica Section B: Structural Science Crystal Engineering Materials 2024; 80: 548-574.

88. Das PP, Andrusenko I, Mugnaioli E, Kaduk JA, Nicolopoulos S, Gemmi M, Boaz NC, Gindhart AM, Blanton TN. Crystal structure of linagliptin hemihydrate hemiethanolate, $(C_{25}H_{28}N_8O_2)_2(H_2O)(C_2H_5OH)$ from 3D electron diffraction data, Rietveld refinement, and density functional optimization. Crystal Growth & Design 2021; 21: 2019-2027.